Selectivity in Fragmentation of N-methylacetamide after Resonant K-shell Excitation

Peter Salén,[a] Magdalena Kamińska,[a,b,c] Richard J. Squibb,[b,d] Robert Richter,[e] Michele Alagia,[f] Stefano Stranges,[f,g] Peter van der Meulen,[a] John H.D. Eland,[h] Raimund Feifel,[b,d] and Vitali Zhaunerchyk*[b,d]

Received Xth XXXXXXXXXX 20XX, Accepted Xth XXXXXXXXX 20XX
First published on the web Xth XXXXXXXXXX 200X
DOI: 10.1039/b000000x

The fragmentation pattern of the peptide model system, N-methylacetamide, is investigated using ion time-of-flight (TOF) spectroscopy after resonant K-shell excitation. Corresponding near-edge X-ray absorption fine structure (NEXAFS) spectra recorded at high resolution at the C1s, N1s and O1s edges are presented. Analysis of the ion TOF data reveals a multitude of fragmentation channels and dissociation pathways. Comparison between the excitation of six different resonances in the vicinity of the C1s, N1s and O1s edges suggests evidence for site-selective bond breaking. In particular the breaking of the peptide bond and the N-C_α bond show a clear correlation with resonant excitation at the N1s edge. Also, stronger tendencies towards site-selective bond breaking are found for the generation of single ions compared with ion pairs. Analysis of angular distributions of ions from breakage of the peptide bond yields a fragmentation time of < 400 fs.

1 Introduction

The development of experimental techniques using X-rays is important for the study of biological molecules. Determination of the geometric structure, which is related to the function of these molecules, can, for instance, be achieved by X-ray crystallography[1]. Spectroscopic techniques such as X-ray photoelectron spectroscopy (XPS) and near-edge X-ray absorption fine structure (NEXAFS) spectroscopy enhance our understanding of the electronic structure[2–8] and give detailed information on the sample composition and its decomposition mechanisms[9,10] which are relevant in respect to the samples' biological function. Since proteins and peptides consist of amino acids linked together by peptide bonds, the investigation of these bonds are of particular interest.

The fragmentation of peptides has been intensively investigated in the past using various activation methods such as black-body radiation[11], infrared multi-photon excitation[12], ultraviolet[13] and vacuum ultraviolet[14] excitation, and collisions with gas-phase molecules or surfaces[15,16]. These measurements typically display cleavage of the weak peptide bond as a consequence of statistical fragmentation where the internal energy is randomized before dissociation occurs. In contrast, more specific bond breaking has been demonstrated using electron capture dissociation and electron transfer dissociation[17,18]. Here the localized excitations resulted in the cleavage of the stronger N-C_α bonds before the energy was distributed throughout the molecule. Furthermore the use of intense femtosecond near infrared laser beams with feedback-optimized pulse shapes has revealed preferential cleavage of specific peptide bonds[19]. This type of control has potential use as a complementary tool for protein sequencing[19].

Soft X-rays are, to some extent, suitable for site-specific bond breaking in molecules due to the localized nature of K-shell excitation. By tuning the wavelength to the K-edge corresponding to a particular atomic element, one may choose which atomic species to excite. Furthermore, by tuning to a site-specific resonance, one may preferentially select the site in the molecule where the 1s hole is created. The K-shell excitation is followed by an Auger decay occurring typically on a $<$10 fs time scale, often leaving the molecule in an excited state. For resonant K-shell excitation the subsequent Auger process can be of the spectator type[20] where the excited core electron remains in an outer valence orbital while another electron from an outer orbital fills the core-hole, ejecting one

[a] *Department of Physics, Stockholm University, 106 91 Stockholm, Sweden.*
[b] *Department of Physics and Astronomy, Uppsala University, 752 21 Uppsala, Sweden.*
[c] *Institute of Physics, Jan Kochanowski University, 25-369 Kielce, Poland.*
[d] *Department of Physics, University of Gothenburg, 412 96 Gothenburg, Sweden.*
[e] *Elettra - Sincrotrone Trieste, Area Science Park, 34149 Basovizza, Trieste, Italy.*
[f] *IOM-CNR Tasc, SS-14, Km 163.5 Area Science Park, Basovizza, I-34149 Trieste, Italy.*
[g] *Dipartimento di Chimica e Tecnologie del Farmaco, Università Sapienza, I-00185 Roma, Italy.*
[h] *Department of Chemistry, Oxford University, Oxford OX1 3QZ, United Kingdom.*
∗ vitali.zhaunerchyk@physics.gu.se.

or more electrons. This yields a singly or multiply charged molecular ion with two or more valence vacancies. It has been suggested that the generated valence vacancies are localized around the atom where the core hole was created, so called Coulomb localization[21], and may subsequently drive dissociation via Coulomb repulsion. Consequently, some memory of the localized excitation might be conserved after the Auger process and if it is even maintained through the dissociation, one could expect to selectively break the bonds around the core excited site.

In respect to preserving the localization of the initial excitation, one may expect a difference between a gas-phase molecule and a molecule attached to bulk material such as a surface or a large cluster. This distinction has been described by a simple model[22] where the memory of the initially localized excitation is weakened for the isolated molecule since the excess energy is distributed throughout the molecule which can lead to statistical fragmentation putatively being dominant. For a molecule adsorbed on a surface, the excess energy instead flows into the surface and thus the statistical fragmentation is reduced and the site-selective bond breaking is enhanced.

The early work of Eberhardt *et al.*[23] suggested some first evidence of site-selective fragmentation by resonantly exciting the C1s electron in gaseous acetone. However, later experiments using O1s resonant core excitation of acetone did not confirm such an atomic site selectivity[24]. Since then, many studies have been performed on this topic in the gas-phase[25–30] as well as on surfaces[22,31–34] and site-specific bond breaking has been observed in both cases. Also, site-specific fragmentation initiated by core ionization has been reported[35–43].

In this paper we present investigations into the fragmentation pattern of N-methylacetamide ($CH_3NHCOCH_3$) and a deuterated version of it using resonant K-shell excitation; the schematic structure of the isotopologues studied are shown in Fig. 1. N-methylacetamide is a small model system of a peptide which contains its key bonds: the peptide bond and the bonds to the C_α carbons on each side of the peptide link through which aminoacids are connected. It is therefore a useful test molecule for studies of bond breaking in peptides. NEXAFS spectra were recorded at high resolution in order to locate pre-edge resonances in the vicinity of the C, N and O edges and in order to study subsequently the fragmentation patterns associated with these resonances using an ion time-of-flight (TOF) coincidence spectroscopy technique. For easier identification of the fragments originating from either side of the molecule the deuterated form of N-methylacetamide ($CD_3NHCOCH_3$) is investigated.

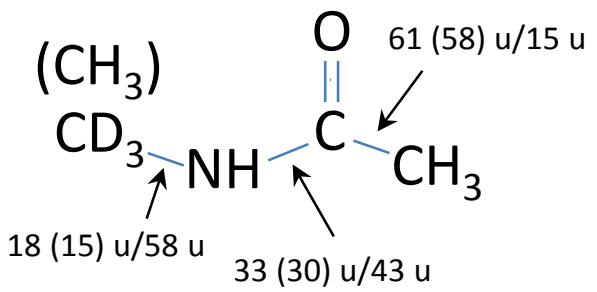

Fig. 1 Schematic structure of deuterated (and non-deuterated) N-methylacetamide with indications of the ion masses, in atomic mass units, to be expected from breakage of the different bonds.

2 Experiment and data analysis

The experiment was performed at the gas-phase photoemission beamline of the Elettra synchrotron radiation facility[44] located at Trieste, Italy. The soft X-ray pulses were generated in an undulator by circulating electron bunches stored in the ring at an energy of 2.0 GeV. The desired photon energy was selected by tuning the undulator gap and the light was monochromatized with a grating combined with a variable slit providing an X-ray photon energy resolution below the core-hole lifetime. The N-methylacetamide was a commercial sample and the content of deuterium atoms in the sample of the deuterated version of the molecule was 99.9%. It was injected into the interaction volume through a needle of internal diameter of 2 mm forming an effusive beam which crossed the X-rays. The sample had sufficiently high vapor pressure at ambient temperatures such that no sample heating was needed.

The charged reaction products, *i.e.* electrons and ions, were detected with a photoelectron-photoion coincidence apparatus[45]. The ion analyser is a Wiley-McLaren type TOF spectrometer with a 32×32 pixel position sensitive anode, allowing for ion momenta measurements[45,46]. The apparatus does not allow measurement of the electron kinetic energy; electrons were detected purely as a time reference for ion coincidence measurements.

In order to estimate the detection efficiency (D_{eff}) of the spectrometer we refer to Fig. 2 which shows the spectra of N-methylacetamide recorded with a photon energy of 320 eV, from single ions (blue line), ion pairs (red line), triple ions (black line), and quadruple ions (green line), (*i.e.* detections of two, three and four coincident ions, respectively, in the three latter cases). Here *m/z* is the mass-to-charge ratio. D_{eff} was determined by solving the equations for the total number of counts of each of the four spectra as a function of D_{eff} and the produced ion pairs, triple ions, and quadruple ions. Since the photon energy is above the C1s ionization limit, doubly or higher charged ions will be created from the formation of

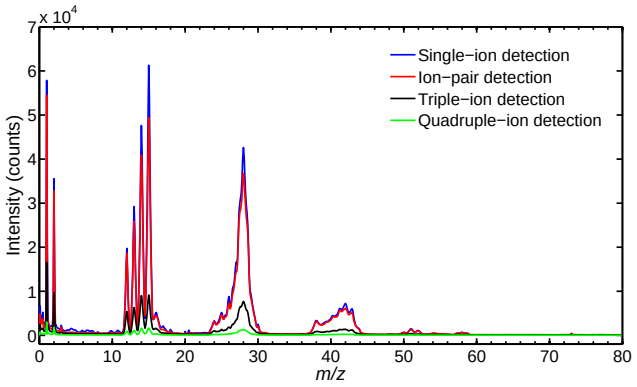

Fig. 2 Ion spectra of N-methylacetamide showing the detection of single ions (blue line), ion pairs (red line), triple ions (black line) and quadruple ions (green line) recorded at a photon energy of 320 eV, *i.e.* above the carbon edge, and plotted on a common scale. Calculations based on the integrated intensities of the spectra reveals a detection efficiency of approximately 38%. The H-peak (m=1 u) has been reduced by a factor of 10.

a core hole and the subsequent Auger decay. Consequently the contribution from single ions has been set to zero in these calculations. Contributions from ions produced by valence ionization have been subtracted for each spectrum. The normalization for this subtraction was performed by matching the intensity of the parent-ion peak for the spectra recorded with 275 eV (which was subtracted) and 320 eV. From this analysis $D_{\text{eff}}\approx$38% was estimated. The interpretation of the ion spectra is explained in more detail in section 3.2.

The ion spectra of this article were recorded at photon energies corresponding to the six resonances as marked by vertical lines in Fig. 3. Additional ion spectra were recorded just below (275 eV, 395 eV and 520 eV) and above (320 eV, 430 eV and 555 eV) the resonances of each absorption edge. Data taken below the resonance was used to subtract the non-resonant contribution from the on-resonance spectra, yielding the pure resonant contribution. The normalization factor for this subtraction was given by setting the intensity of the Ar^{2+} peak at m/z=20 equal in both cases. This peak originates from residual Argon in the chamber. Since the Argon-ionization cross section is similar for the two photon energies (on-resonance and just below the resonance), a normalization to equal intensity of the Ar^{2+} peak ensures equivalent total exposure. The data above the resonances was used for comparison with the resonant data. Corrections were applied to account for the fact that the 38% detection efficiency will result in false contribution of fewer ions detected than actually created (*e.g.* single ions will be detected from the generation of ion pairs). This correction included the contribution from up to four ions created. All spectra have been binned by 0.1 u, where u is the atomic mass unit. Below we will use the mass, m, instead of m/z, when referring to the peaks of the figures, because, except for Ar^{2+}, we only detect singly charged ion fragments.

The spectrum with 402.1 eV excitation showed some signs of residual N_2 in the chamber from a previous pure N_2 measurement. This was indicated by slightly stronger peaks at m=14 u (N_2^{2+}, N^+) and 28 u (N_2^+) in the spectrum. Hence, these peaks were excluded in the integrated intensities of the spectra used for normalization with respect to different excitation energies, for all excitation energies.

3 Results and Discussion

3.1 NEXAFS spectra

In order to determine the energies of various K-shell resonances in the vicinity of the C, N and O-edges of N-methylacetamide, NEXAFS spectra were recorded. Fig. 3 shows these NEXAFS spectra for non-deuterated N-methylacetamide, where the vertical lines indicate the resonances subsequently investigated. The corresponding spectra for the deuterated molecule are very similar. The spectra have been normalized by dividing by the Argon-ion signal. Below 286 eV the contamination of the optics is strongly affecting the normalization and therefore the spectrum of Fig. 3a is plotted above this value.

Calculated NEXAFS spectra for N-methylacetamide have, to the best of our knowledge, been reported only for the N and O edges[47] and predicted rough similarities. Although a detailed assignment of the spectral structures cannot be performed on the basis of previous investigations of this molecule, studies of similar molecules[3–5,7] suggest that the dominant peak in each NEXAFS spectrum is associated with a 1s$\rightarrow\pi^*$ transition.

3.2 Fragmentation patterns

Fragmentation patterns of both N-methylacetamide and its deuterated form were measured consistently at the six resonant photon energies marked in Fig. 3 using an ion TOF coincidence set-up. However, in what follows we mostly focus on the spectra of the deuterated molecule since it allows easier identification and time-separation of the different fragments. The non-deuterated form serves for cross-checks and confirmation.

Fig. 4 displays the all-ions mass spectrum corresponding to excitation of the strongest C-resonance at 289 eV with peak assignments. The blue line represents the spectrum of the deuterated molecule (m=76 u) and the red line the non-deuterated (m=73 u) isotopologue. The peak assignments are not complete and serve mainly as guidance for the discussion below.

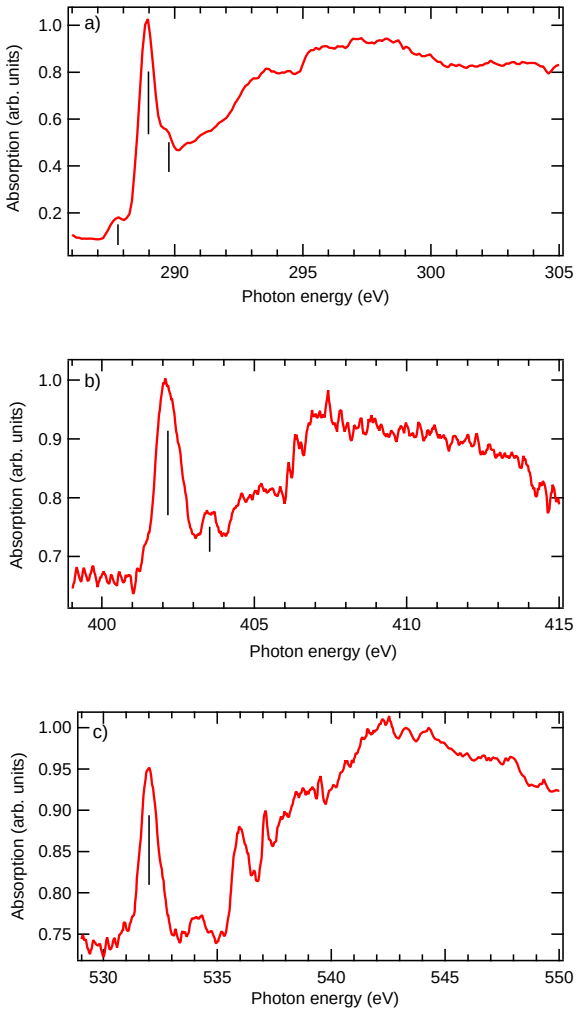

Fig. 3 Total-ion yield NEXAFS spectra of N-methylacetamide recorded in the vicinity of the a) C1s , b) N1s and c) O1s edges. The vertical lines indicate the resonances investigated.

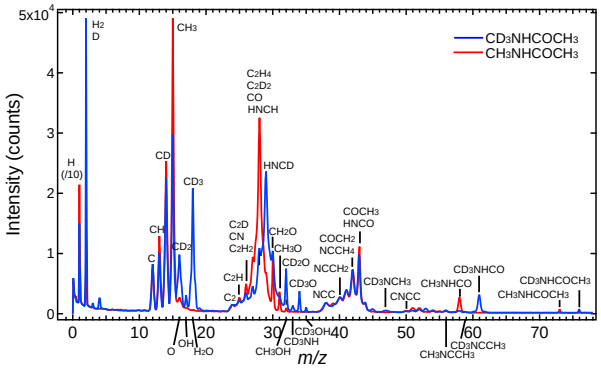

Fig. 4 Ion spectra of N-methylacetamide (red line) and deuterated N-methylacetamide (blue line) recorded at 289 eV photon energy with peak assignments. The H-peak (*m*=1 u) has been reduced by a factor of 10.

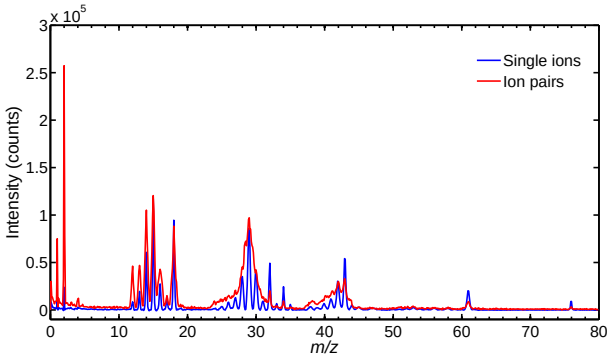

Fig. 5 Ion spectra of deuterated N-methylacetamide corresponding to the creation of single ions (blue line) and ion pairs (red line). The data were obtained at 289 eV photon energy. The H-peak (*m*=1 u) has been reduced by a factor of 10.

The identification of the peaks ranging from *m*=1 u to *m*=20 u is quite straightforward. This spectral region is dominated by hydrogen and the methyl groups and the corresponding groups for the deuterated molecule. For *m*=27 u to *m*=35 u a comparison of the spectra from the two isotopologues is helpful in assigning the peaks. For example, the peak at *m*=28 u in the spectrum of the non-deuterated, and at 29 u in the spectrum of the deuterated compound, is highly pronounced, which suggests this peak being mainly associated with $HNCH^+$ and $HNCD^+$. Furthermore, the assignments of CD_2O^+ and CD_3O^+ are assisted by the corresponding peaks, CH_2O^+ and CH_3O^+, in the spectra of the non-deuterated molecule. In the region between *m*=38 u and *m*=44 u, the similarity between the two spectra indicates fragments free of D. Note the peaks associated with the breaking of the peptide bond at *m*=33 u and *m*=43 u in the blue spectrum. At higher values of *m* the most intense features at *m*=58 u and *m*=61 u originate from the fragments which correspond to breaking the C_α bonds. The general appearance of the spectra suggests that a lot of different fragments are produced and that there is a relatively high probability for multiple bonds to be broken, generating fragments such as C_2^+, NCC^+ and $CNCC^+$.

Fig. 5 shows spectra of single ions and ions in pairs at the photon energy of 289 eV. From Fig. 5 it can be seen that the spectral peaks are broader for the ion pairs (red) than the single ions (blue). This is expected since they are formed from doubly charged ions, as opposed to the singly charged parent ions, and therefore the kinetic energy release is larger.

3.2.1 Fragmentation of singly charged ions. Fig. 6 shows ion TOF spectra which reflect the fragmentation pattern of singly charged deuterated N-methylacetamide. In or-

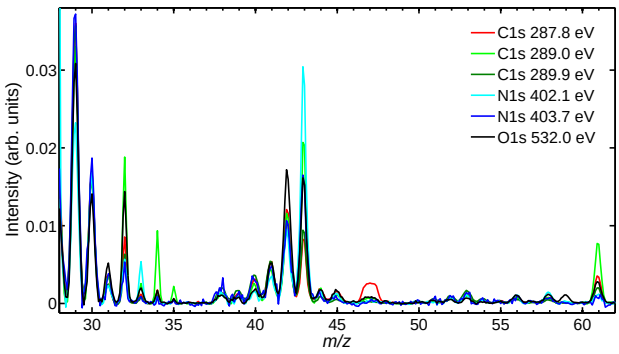

Fig. 6 Spectra of single ions of deuterated N-methylacetamide upon excitation at the different photon energies. Each spectrum is normalized to its integrated intensity in order to illustrate the spectral differences for the different excitation energies.

der to illustrate the differences between the spectra recorded at various resonances, the spectra are superimposed after having been normalized to the total number of counts for each spectrum. Many differences between various resonant excitations are found in the range between *m*=28 u and *m*=62 u and therefore only this region is shown in Fig. 6. Table 1 lists the relative yields for a selected choice of relevant masses, allowing for a more quantitative comparison. These values have been obtained by calculating the integrated area in Fig. 6 for *m* ranging from *m*-0.5 u to *m*+0.5 u. Bold fonts are used to highlight the values with the most pronounced difference compared to the same *m* at different resonance conditions.

Beginning from the low-*m* region of the spectra, the first pronounced difference can be observed at *m*=33 u, where the lowest N1s resonance located at about 402.1 eV has a strong peak. This *m* corresponds to the lighter fragment (CD_3NH^+) generated when breaking the central (N-C) peptide bond. The other fragment has *m*=43 u ($COCH_3^+$) and this peak is also strongest for the N1s 402.1 eV resonance. This indicates an increased probability of breaking the peptide bond at this photon energy, although it should be noted that *m*=43 u also may have contributions from $HNCO^+$.

Another peak stands out at *m*=34 u, which corresponds to the CD_3O^+ fragment formed by rearrangement. The abundance of this ion is markedly higher for the C1s 289 eV resonance. We observe a similar trend for *m*=32 u and *m*=35 u, which correspond to CD_2O^+ and CD_3OH^+, respectively.

m=58 u and *m*=61 u correspond to the fragments formed when the CD_3 or CH_3 group is detached. As can be seen from Table 1 the ratio between the yields of these fragments, (*m*=61 u)/(*m*=58 u), is only less than 1 for the case of the N1s resonances. This suggests that by resonant excitation at the atom directly connected to it, CD_3 is more likely to be detached than the distant CH_3. Furthermore, excitation at 402.1 eV results in the highest yield of fragments of *m*=58 u, *i.e.* at this resonance one is most likely to detach only CD_3.

m=59 u has a significant contribution to the spectra only at the O1s 532 eV resonance. This peak can be assigned to $CD_3NCCH_3^+$, which corresponds to the detachment of OH from the parent ion. From the weak signal at *m*=60 u, one may conclude that the removal of a single O-atom is unlikely when compared to the detachment of OH.

From these observations, we note that the N1s 402.1 eV resonance is more likely to break the peptide bond as well as the N-C_α bond in comparison to the other resonances. In both cases, the bonds which are preferentially broken when exciting at the N1s 402.1 eV resonance are located next to the N-atom. Hence, these results can be considered as a manifestation of site-selective bond breaking. We note that this behavior is not seen when the nitrogen 1s core electron is ejected into the continuum.

3.2.2 Fragmentation of doubly charged ions. Doubly charged parent ions will break mainly into two singly charged ions. A comparison of the mass spectra measured at the different resonances, similar to Fig. 6 but for the detection of ion pairs instead of single ions, is shown in Fig. 7. The difference in intensity of the peaks between the various excitation energies are generally larger in Fig. 6 than in Fig. 7. Therefore these figures seem to indicate that selection of single ions rather than ion pairs reveals more pronounced differences in response between the resonances. However, because many peaks in the ion-pair spectra of Fig. 7 are broad, overlaps would add severely to uncertainty in the integrated intensity of the peaks. Hence, instead of integrating the intensity of the mass spectral peaks as was done for single ions in Table 1, we seek a more accurate quantitative estimate of the relative yields of ion pairs from 2-dimensional coincidence maps, where competing contributions are separated.

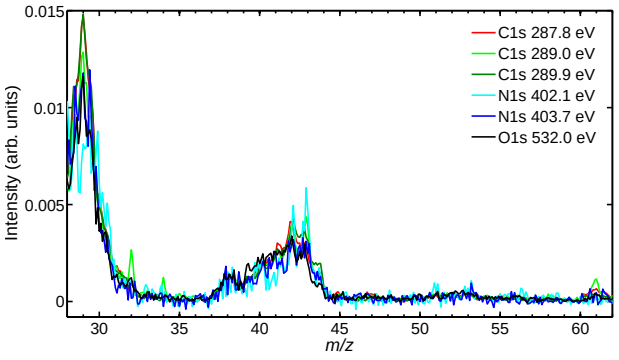

Fig. 7 Spectra of ion pairs of deuterated N-methylacetamide upon excitation at the different photon energies. Each spectrum is normalized to its integrated intensity in order to illustrate the differences in spectral appearance for the different excitation energies.

Table 1 Relative yields (%) of single ions of deuterated N-methylacetamide at different excitation energies, *E*. The bold numbers highlight values that stand out compared to other resonances of the same *m*. The error margins are statistical uncertainties.

m (u)	*E*=287.8 eV	*E*=289.0 eV	*E*=289.9 eV	*E*=402.1 eV	*E*=403.7 eV	*E*=532.0 eV
15	6.1 ± 0.2	9.7 ± 0.1	8.4 ± 0.2	12 ± 2	12 ± 4	14 ± 2
18	9.7 ± 0.2	8.7 ± 0.1	6.6 ± 0.1	6.4 ± 1.6	7.8 ± 2.8	10 ± 2
33	0.45 ± 0.03	0.79 ± 0.03	0.27 ± 0.02	**1.8 ± 0.1**	0.33 ± 0.12	0.79 ± 0.06
34	0.47 ± 0.02	**2.2 ± 0.1**	0.32 ± 0.02	0.23 ± 0.06	0.00 ± 0.09	0.48 ± 0.05
43	3.8 ± 0.2	8.1 ± 0.1	4.4 ± 0.1	**15 ± 1**	7.8 ± 1.0	7.3 ± 0.5
47	**2.4 ± 0.1**	0.58 ± 0.02	0.21 ± 0.02	0.30 ± 0.04	0.25 ± 0.07	0.73 ± 0.04
58	0.48 ± 0.02	0.43 ± 0.02	0.30 ± 0.02	**0.92 ± 0.04**	**0.47 ± 0.06**	0.73 ± 0.03
59	0.08 ± 0.01	0.12 ± 0.02	0.06 ± 0.01	0.14 ± 0.03	0.02 ± 0.04	**0.68 ± 0.02**
61	1.8 ± 0.1	3.6 ± 0.1	1.1 ± 0.1	**0.70 ± 0.08**	**0.43 ± 0.15**	1.5 ± 0.1

Coincidence maps show pairs of correlated ions and, thus give the probability of formation of two specific fragments from the same parent molecule. Fig. 8 presents the coincidence map for the C1s 289 eV resonance and Figs. 9a-f display zoomed-in regions as marked in Fig. 8 with red rectangles. Relative intensities of various coincidence peaks were found in a similar way as for the mass spectra, i.e. by integrating peak volumes, subtracting below-resonance contributions and then normalizing to the total number of coincidence counts.

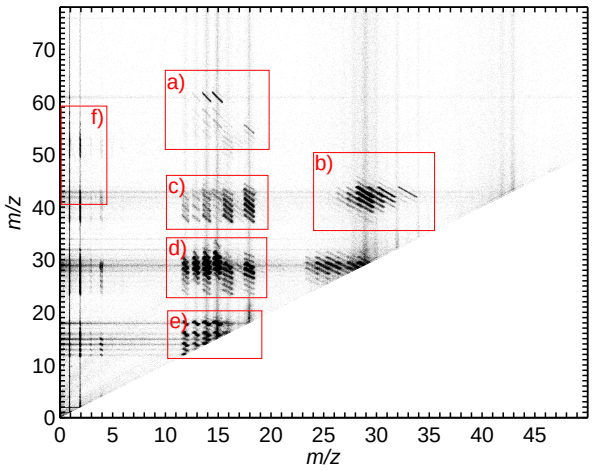

Fig. 8 Coincidence map for 289 eV excitation of deuterated N-methylacetamide. The red rectangles represent zoomed-in regions displayed in Fig. 9.

The single-ion data show a higher probability at the two N1s resonances for detaching neutral CD_3· rather than CH_3·, as indicated by the smaller (*m*=61 u)/(*m*=58 u) intensity ratio, about 0.8 there as against about 3 at lower photon energies. For ion pairs the coincidence map Fig. 9a shows that the CD_3^+ ion (*m*=18 u) correlates mainly with fragments of *m*=55 u, so the creation of the CD_3^+ fragment is accompanied by loss of three hydrogen atoms (or H_2 and H fragments). Hence, to compare the detachment of CD_3^+ or CH_3^+ ions from doubly charged parents, we examine the intensity ratio of *m*=61 u and *m*=55 u. In Table 2 one can see that this ratio shows the same trend as for the single ions of an increased probability for detachment of CD_3^+ compared with CH_3^+ at the N1s resonances, especially at 402.1 eV. A few other coincidence peak intensities are included in Table 2. Comparison of the ion intensities in Table 1 with the pair intensities in Table 2 at the different resonance energies suggests that site-specific fragmentation is more pronounced when single ions are created rather than ion pairs, at least with respect to breaking of the peptide bond.

In addition to intensities, the shape and slope of the coincidence peaks contain important information on the fragmentation mechanism[48]. Since the non-resonant contributions to the data measured at the resonance of 289 eV are small compared to those at other NEXAFS peaks, the shapes of the coincidence peaks are analyzed only for this resonance. Figs. 9a-f show evidence of secondary fragmentation involving multistep mechanisms (see Table 3), but to focus the present discussion we concentrate mainly on simple breakages of the peptide and C_α bonds. The intensities of the relevant coincidence peaks are listed in Table 4, together with the intensities of the tail features shown in Fig. 9f, which are discussed further below.

The coincidence peaks associated with the breaking of the C_α bonds, when the rest of the molecular skeleton (NCOC or CNCO) does not fragment, are shown in Fig. 9a. It follows from this scheme that the creation of the CD_3^+ fragment, as mentioned before, is accompanied by loss of three hydrogen atoms (or H_2 and H fragments), while in the $[CD_3NHCO–CH_3]^{++}$ bond breakage the heavier ion fragment remains intact but one hydrogen atom can be detached from the methyl group. The strong 61-15 and 61-14 coincidence peaks show that either CH_3^+ (*m*=15 u) or CH_2^+ (*m*=14 u) can be formed together with CD_3NHCO^+ (*m*=61 u). Furthermore, Fig. 9a illustrates the site preference for the C_α-bond cleavage when ruptures of other bonds between heavy atoms do not occur;

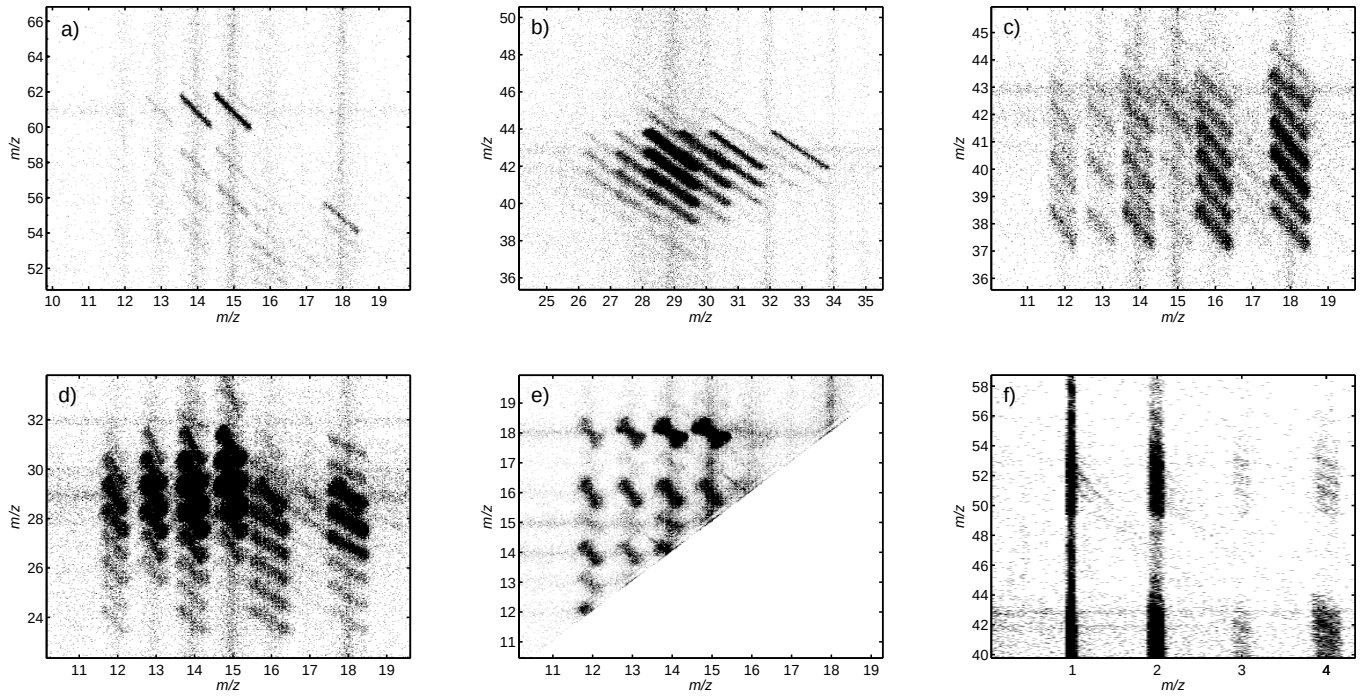

Fig. 9 Zoomed-in regions of the coincidence map corresponding to the red rectangles of Fig. 8, from measurements at the C1s 289 eV resonance, save for Fig. 9f which was measured at the N1s 402.1 eV resonance.

Table 2 Relative yields (%) of ion pairs of deuterated N-methylacetamide for different excitation energies, E. These values are obtained by adding the most intense coincidence peaks, shown in parenthesis, of a specific mass (m_1). The error margins are statistical uncertainties.

m (u)	E=287.8 eV	E=289.0 eV	E=289.9 eV	E=402.1 eV	E=403.7 eV	E=532.0 eV
33 (m_1=33-m_2=15,43)	0.31 ± 0.02	0.21 ± 0.01	0.24 ± 0.01	0.25 ± 0.02	0.18 ± 0.02	0.24 ± 0.02
43 (m_1=43-m_2=14,15,16,18,28,29,30,31,33)	5.1 ± 0.1	3.7 ± 0.1	6.3 ± 0.1	5.0 ± 0.2	4.4 ± 0.2	2.3 ± 0.3
55 (m_1=55-m_2=18)	0.11 ± 0.01	0.056 ± 0.001	0.059 ± 0.002	0.17 ± 0.01	0.16 ± 0.01	0.041 ± 0.004
61 (m_1=61-m_2=14,15)	1.0 ± 0.1	0.38 ± 0.01	0.60 ± 0.01	0.17 ± 0.07	0.42 ± 0.06	0.15 ± 0.05

Table 3 Reactions (a1) to (e2), where the letter refers to the sub-figures ordering of Fig. 9, illustrating the multitude of possible fragmentation pathways. It may stop after dissociation into two major fragments as in (a1), (a2) and (b1), or dissociate further after initial detachment neutral components as in (b2) and (c3), or different ions as in (c1), (c2), (d1), (e1) and (e2). The question mark in (e1) and (e2) indicates that it is unclear how NHCO splits up.

$$
\mathrm{CD_3NHCOCH_3^{2+}} \longrightarrow \begin{cases}
\mathrm{CD_3NHCO^+ + CH_3^+} & \text{(a1)} \\
\mathrm{CD_3^+ + NHCOC^+ + 3H} & \text{(a2)} \\
\mathrm{CD_3NH^+ + COCH_3^+} & \text{(b1)} \\
\mathrm{CD_zNH_yCOCH_x^{2+} + (3-z)D + (1-y)H + (3-x)H \rightarrow CD_zNH_y^+ + COCH_x^+ + (3-z)D + (1-y)H + (3-x)H} & \text{(b2)} \\
\mathrm{CD_3^+ + NHCOCH_3^+ \rightarrow CD_3^+ + NHCO^+ + CH_3} & \text{(c1)} \\
\mathrm{CD_3^+ + NHCOCH_3^+ \rightarrow CD_3^+ + COCH_3^+ + NH} & \text{(c2)} \\
\mathrm{CD_3NCCH_v^{2+} + O + (4-v)H \rightarrow CD_3^+ + NCCH_v^+ + O + (4-v)H} & \text{(c3)} \\
\mathrm{CD_3NCH_3^+ + COH^+ \rightarrow CD_3^+ + COH^+ + NCH_3} & \text{(d1)} \\
\mathrm{CD_z^+ + NHCOCH_x^+ + H_{3-x} + D_{3-z} \rightarrow\ CD_z^+ + CH_x{}^+ + NHCO(?) + H_{3-x} + D_{3-z}} & \text{(e1)} \\
\mathrm{CD_zNHCO^+ + CH_x^+ + H_{3-x} + D_{3-z} \rightarrow\ CD_z^+ + CH_x^+ + NHCO(?) + H_{3-x} + D_{3-z}} & \text{(e2)}
\end{cases}
$$

where v=0-4, x=0-3, y=0-1 and z=0-3.

Table 4 Intensities of coincidence peaks normalized to the total coincidence counts, and multiplied by 1000, for deuterated N-methylacetamide at different excitation energies. Coincidence detection of fragments of *m*=*x* u and *m*=*y* u is denoted by *x*-*y*. The last two columns correspond to the intensities of the tails originating from the coincidence peak marked in the column title. The error margins are statistical uncertainties.

Excitation energy	61-15	55-18	43-33	52-1 (tail)	53-1 (tail)
275.0 eV	14 ± 1	0.60 ± 0.02	7.1 ± 0.1	0.07 ± 0.01	0.08 ± 0.01
287.8 eV	5.7 ± 0.2	1.1 ± 0.1	1.7 ± 0.1	0.08 ± 0.03	0.14 ± 0.02
289.0 eV	2.5 ± 0.1	0.56 ± 0.01	1.2 ± 0.1	0.07 ± 0.04	0.11 ± 0.01
289.9 eV	4.0 ± 0.1	0.59 ± 0.02	1.3 ± 0.1	0.09 ± 0.01	0.13 ± 0.02
402.1 eV	0.7 ± 0.7	1.7 ± 0.1	1.8 ± 0.2	0.05 ± 0.05	0.20 ± 0.06
403.7 eV	3.3 ± 0.5	1.6 ± 0.1	1.1 ± 0.2	0.03 ± 0.04	0.10 ± 0.03
532.0 eV	0.8 ± 0.5	0.41 ± 0.04	1.6 ± 0.2	0.10 ± 0.03	0.25 ± 0.04
555.0 eV	1.1 ± 0.4	0.21 ± 0.03	2.0 ± 0.2	0.08 ± 0.02	0.18 ± 0.02

breakage of the CH_3-CO linkage is more likely than CD_3-NH breakage on the other site of the molecule. This is especially noticeable when the remaining part of the molecule is an intact ion, as evidenced by the weak peak at 58-18 compared with that at 61-15. The correlation peaks in Fig. 9a are all narrow bars of slope -1, which is characteristic of breakup resulting in two equally charged fragments. Although the 55-18 correlation peak is not associated with a two-body breakup, the H atoms are light and if they are released with low momentum the peak will have a shape similar to those from two-body break-up[48].

The coincidence peaks associated with cleavage of the peptide bond are shown in Fig. 9b. All the peaks shown in this figure have a slope near -1. The 43-33 peak that corresponds to the peptide bond rupture with no additional fragmentation is a narrow bar, while the other intense peaks are broader because some kinetic energy is released in secondary fragmentation. These observations indicate that loss of neutral hydrogen or deuterium fragments occurs before breakage of the peptide bond itself.

In Fig. 9c it is striking that the peaks representing fragments from secondary decay (m=38-43 u) correlated with CD_3^+ ions (m=18 u) are significantly more intense than those correlated with CH_3^+ ions (m=15 u). This is opposite to the behaviour seen when the complementary ions remain intact, as discussed above. From the peaks correlating to m=18 u in Fig. 9c, reactions (c1)-(c3) of Table 3 are extracted and are justified by their slopes. The slope for the type of two-step decay where the heavier ion is formed in the second step, as in (c1) and (c2), is expected to be $-m_{hi}/(m_{hi}+m_n)$, where m_{hi} and m_n are the masses of the heavier ion and the neutral fragment, respectively[48]. The 43-18 correlation peak has a slope of approximately -0.75 which is close to the predicted value of -0.7 given by this formula and thus suggests that this peak is associated with reactions (c1) and (c2). The peaks showing correlations between m=38-42 u and m=18 u have slopes of -1 which points to reactions where a neutral is initially detached[48], as in reaction (c3).

Fig. 9d shows many overlapping features with different slopes and shapes reflecting the fact that the break-up processes may proceed via distinct dissociation routes to the same final products. The multitude of peaks makes a detailed description of the processes contained in this figure difficult. However, reaction (d1) of Table 3 is extracted from the peak which has the steeper slope of the two contributions at 29-18. The slope of this peak is -2 which fits well with a two-step decay where the lighter ion is formed in the second step, in which case the peak should have a slope of $-(m_{li}+m_n)/m_{li}$, where m_{li} is the mass of the lighter ion[48].

The peaks associated with the formation of two methyl ions (or possibly NH^+), and those where different numbers of H atoms have been lost from the C_1 fragments are shown in Fig. 9e. Two significantly different slopes within each peak, especially visible at correlations with m=18 u, suggest that the peaks are associated with the initial detachment of either the CH_x^+ or the CD_z^+ ion, where x=0-3 and z=0-3, as in reactions (e1) and (e2) of Table 3. The slopes at the 18-15 correlation are -0.3 and -2.5. The former fits well with the expected value of -0.35 for a reaction of type (e2), while the latter is somewhat higher than the anticipated value of -3.9 for a reaction of type (e1).

Fig. 9f exhibits faint tail structures originating at 52, 53-1 and extending towards smaller m on the y-axis and larger m on the x-axis. These tails are a sign of metastable doubly-charged ions which undergo a delayed fragmentation as they propagate through the TOF tube[46,49]. The properties of the instrument imply that the lifetime of these metastable states are longer than 50 ns[46,49]. The integrated tail intensities listed in Table 4 reveal a propensity for increased abundance at the O1s 532 eV resonance. Formation of the metastable $CNCCH_3^{2+}$ and $CNHCCH_3^{2+}$ ions requires the removal of the oxygen atom from the parent molecule and, thus, this is possibly another example of selective bond breaking.

Finally we note that since the fragmentation is closely connected with the Auger decay, deeper insights into the fragmentation processes would be given by electron coincidence measurements which provide information about the correlation between the fragmentation and electronic decay. The results of the present article however shows that useful information can already be extracted from pure ion coincidences and it should serve as a good starting point for further studies.

3.3 Angular distribution and kinetic energy release.

The position and time sensitive detection of the ion fragments permits the β-parameter[50] to be determined from the angular distribution, as well as the kinetic energy release (KER). We focus on the C1s 289 eV resonance here because it has negligible below-resonance contributions. We also restrict ourselves to the two-body break-up channels.

The β-parameter can be extracted from the angular distribution of the detected ions. This distribution may be expressed as[51]

$$I(\theta)\sin(\theta) = \frac{\sigma_{tot}}{4\pi}\left(1+\frac{\beta}{2}(3\cos^2\theta-1)\right) \qquad (1)$$

where θ is the angle between the electric field vector of the linearly polarized X-rays and the velocity vector of the fragment ion. $I(\theta)$ and σ_{tot} denote the differential and total cross-sections, respectively. The angular distribution of the ions generated upon the breaking of the peptide bond (reaction (b1)) of deuterated N-methylacetamide is displayed in Fig. 10, from which a value of β=-0.56 $\pm$ 0.06 was obtained. Accordingly, the fragmentation channel associated with the detach-

ment of the CH_3^+ ion (reaction (a1)) resulted in β=-0.56 $\pm$ 0.08. From the β-parameter, one may learn about the dissociation time, τ, of the parent ion since a longer τ will result in a more isotropic angular distribution due to rotational randomization. This is expressed by the following formula for a pseudo diatomic molecule where each fragment is reduced to a mass point located on the bond axis to be broken:[50]

$$\beta = P_2(\cos\chi)(\frac{1}{2} + \frac{3}{2}\gamma e^{\gamma}\int_{\gamma}^{\infty}\frac{e^{-\nu}}{\nu}d\nu) \quad (2)$$

Here $P_2(\cos\chi)$=$\frac{1}{2}$(3cos$^2\chi$-1), where χ is the angle between the transition moment and the direction of dissociation, γ=$\frac{I}{8kT\tau^2}$, where the temperature T=300 K, k is the Boltzmann constant and I=2·10^{-45} kg·m^2 is the moment of inertia for the molecule. I is an estimate based on the related propanamide molecule[52]. From Eq. 2 we can extract an upper limit of τ=400 $\pm$ 140 fs for the two dissociation channels revealing β=-0.56.

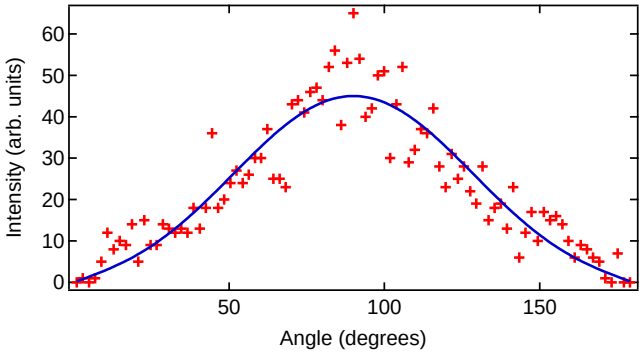

Fig. 10 Angular distribution of the two ions created upon the breaking of the peptide bond in deuterated N-methylacetamide (red markers), including a fit according to Eq. 1 (blue line).

The kinetic energy release distribution of the fragments corresponding to reaction (b1) at 289 eV excitation is shown in Fig. 11. A gaussian fit results in KER=4.48 $\pm$ 0.03 eV for the peptide bond breaking and KER=4.67 $\pm$ 0.01 eV for the detachment of the methyl group. Similar values are found for all other resonances (although they may be affected by below-resonance contributions). This is an indication of a coulomb-explosion driven fragmentation where the KER is not dependent on energy differences in the dissociation curves.

3.4 Conclusions.

NEXAFS and ion spectra were recorded for N-methylacetamide ($CH_3NHCOCH_3$) and its deuterated isotopologue ($CD_3NHCOCH_3$). To begin with, it was not obvious whether excitations at different resonances will lead

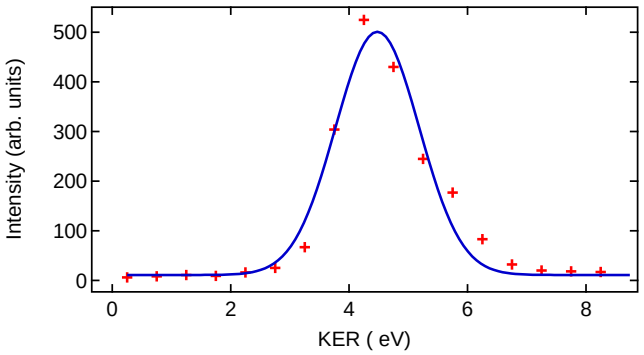

Fig. 11 KER distribution of the two ions formed from deuterated N-methylacetamide after the peptide bond is broken (red markers) including a Gaussian fit (blue line).

to differences in the fragmentation patterns of the molecules, since the excited molecule is likely to relax into many different states and the memory of initially distinct excitations may be washed out.

However, comparison of fragmentation patterns upon excitation of several resonances in the vicinity of the C1s, N1s and O1s edges revealed pronounced differences and indications of site-selective bond breaking. A separation of the ion spectra into those generating single ions or ion pairs showed a stronger tendency towards selective bond breaking when producing single ions. In particular it was demonstrated that excitation of the strongest N1s resonance significantly increases the probability of breaking the bonds connected with the N-atom site, the N-C_α and the peptide bond. Further evidence for site-selective bond breaking was found in an increased probability of removing the OH group at the O1s resonance.

The analysis of the ion-coincidence data revealed complex fragmentation patterns with a multitude of fragmentation channels and dissociation pathways. For example, evidence was found for the generation of metastable states, rearrangement of the parent ion before fragmentation, and various paths of dissociation such as initial detachment of one doubly charged or two singly charged ions which then either dissociates further or stops.

Selectivity in fragmentation is found for simple bond breaking with $<$ 400 fs lifetime, but surprisingly also in metastable ion decays on $>$ 50 ns time scale.

Acknowledgments

This work has been financially supported by the Swedish Research Council and the Knut and Alice Wallenberg Foundation, Sweden. M.K. gratefully acknowledges support from the Swedish Institute.

References

1 A. Yonath, *Current Opinion in Structural Biology*, 2011, **21**, 622-626.

2 K. Kaznacheyev, A. Osanna, C. Jacobsen, O. Plashkevych, O. Vahtras, H. Ågren, V. Carravetta and A.P. Hitchcock, *J. Phys. Chem. A*, 2002 **106**, 3153-3168.

3 Y. Zubavichus, A. Shaporenko, M. Grunze and M. Zharnikov, *J. Phys. Chem. A. Lett.*, 2005, **109**, 6998-7000.

4 J. Stewart-Ornstein, A.P. Hitchcock, P. Hernández Cruz, P. Henklein, J. Overhage, K. Hilpert, J.D. Hale and R.E. Hancock, *J. Phys. Chem. B*, 2007, **111**, 7691-7699.

5 W. Zhang, V. Carravetta, O. Plekan, V. Feyer, R. Richter, M. Coreno and K.C. Prince, *J. Chem. Phys.*, 2009, **131**, 035103-1-11.

6 Y. Zubavichus, A. Shaporenko, M. Grunze and M. Zharnikov, *Nucl. Instr. Methods Phys. Res. A*, 2009, **603**, 111-114.

7 V. Feyer, O. Plekan, R. Richter, M. Coreno, K.C. Prince and V. Carravetta, *J. Phys. Chem. A*, 2009, **113**, 10726-10733.

8 A.R. Milosavljevic, F. Canon, C. Nicolas, C. Miron, L. Nahon and A. Giuliani, *J. Phys. Chem. Lett.*, 2012, **3**, 1191-1196.

9 Y. Zubavichus, O. Fuchs, L. Weinhardt, C. Heske, E. Umbach, J.D. Denlinger and M. Grunze, *Radiation Research*, 2004, **161**, 346-358.

10 P. S. Johnson, P. L. Cook, X. Liu, W. Yang, Y. Bai, N.L. Abbott and F.J. Himpsel, *J. Chem. Phys.*, 2011, **135**, 044702-1-9.

11 W.D. Price, P.D. Schnier and E.R. Williams, *Anal. Chem.*, 1996, **68**, 859-866.

12 J.A. Zimmerman, C.H. Watson and J.R. Eyler, *Anal. Chem.*, 1991, **63**, 361-365.

13 W.D. Bowers, S.S. Delbert, R.L. Hunter and R.T. McIver Jr., *J. Am. Chem. Soc.*, 1984, **106**, 7288.

14 M.S. Thompson, W. Cui and J.P. Reilly, *Angew. Chem. Int. Ed.*, 2004, **43**, 4791-4794.

15 D.F. Hunt, W.M. Bone, J. Shabanowitz, J. Rhodes and J.M. Ballard, *Anal. Chem.*, 1981, **53**, 1704-1706.

16 E.R. Williams, K.D. Henry, F.W. McLafferty, J. Shabanowitz and D.F. Hunt, *J. Am. Soc. Mass Spectrom.*, 1990, **1**, 413-416.

17 R.A. Zubarev, N.L. Kelleher and F.W. McLafferty, *J. Am. Chem. Soc.*, 1998, **120**, 3265-3266.

18 J.E.P. Syka, J.J. Coon, M.J. Schroeder, J. Shabanowitz and D. F. Hunt, *Proc. Natl. Acad. Sci. USA* 2004, **101**, 9528-9533.

19 T. Laarmann, I. Shchatsinin, P. Singh, N. Zhavoronkov, M. Gerhards, C. P. Schulz and I. V. Hertel, *J. Chem. Phys.*, 2007, **127**, 201101-1-4.

20 D.B. Thompson, D.J. Kaidee Lee, C.I. Ma and D.M. Hanson, *J. Phys. B: At Mol. Opt. Phys.*, 1999, **32**, 2649-2666.

21 D.M. Hanson, *Adv. Chem. Phys. vol LXXVII*, John Wiley and Sons Inc., 1990.

22 S. Wada, H. Kizaki, Y. Matsumoto, R. Sumii and K. Tanaka, *J. Phys.: Cond. Matt.*, 2006, **18**, S1629-S1653.

23 W. Eberhardt, T.K. Sham, R. Carr, S. Krummacher, M. Strongin, S. L. Weng and D. Wesner, *Phys. Rev. Lett.*, 1983, **50**, 1038-1041.

24 M. C. Nelson, J. Murakami, S. L. Anderson and D. M. Hanson, *J. Chem. Phys.*, 1987, **86**, 4442-4445.

25 X.J. Liu, G. Prümper, E. Kukk, R. Sankari, M. Hoshino, C. Makochekanwa, M. Kitajima, H. Tanaka, H. Yoshida, Y. Tamenori and K. Ueda, *Phys. Rev. A*, 2005, **72**, 042704-1-5.

26 A. Naves de Brito, R. Feifel, A. Mocellin, A.B. Machado, S. Sundin, I. Hjelte, S.L. Sorensen and O. Björneholm, *Chem. Phys. Lett.*, 1999, **309**, 377-385.

27 A. Naves de Brito, S. Sundin, R.R. Marinho, I. Hjelte, G. Fraguas, Gejo T, Kosugi N, Sorensen S and O. Björneholm, *Chem. Phys. Lett.*, 2000, **328**, 177-187.

28 K. Ueda, M. Simon, C. Miron, N. Leclercq, R. Guillemin, P. Morin and S. Tanaka, *Phys. Rev. Lett.*, 1999, **83**, 3800-3803.

29 P. Erman, A. Karawajczyk, E. Rachlew, M. Stankiewicz and K.Y. Franzen, *J. Chem. Phys.*, 1997, **107**, 10827-10828.

30 P. Morin, M. Simon, C. Miron, N. Leclercq, E. Kukk, J.D. Bozek and N. Berrah, *Phys. Rev. A*, 2000, **61**, 050701-1-4.

31 Y. Baba, *Low Temp. Phys.*, 2003, **29**, 228-242.

32 M.C.K. Tinone, K. Tanaka, J. Maruyama, N. Ueno, M. Imamura and N. Matsubayashi, *J. Chem. Phys.*, 1994, **100**, 5988-5995.

33 E. Ikenaga, K. Kudara, K. Kusaba, K. Isari, S.A. Sardar, S. Wada, K. Mase, T. Sekitani and K. Tanaka, *J. Electron Spectrosc. Relat. Phenom.*, 2001, **114-116**, 585-590.

34 E.O. Sako, Y. Kanameda, E. Ikenaga, M. Mitani, O. Takahashi, K. Saito, S. Iwata, S. Wada, T. Sekitani and K. Tanaka, *J. Electron Spectrosc. Relat. Phenom.*, 2001, **114-116**, 591-596.

35 J.H.D. Eland, P. Linusson, M. Mucke and R. Feifel, *Chem. Phys. Lett.*, 2012, **548**, 90-94.

36 H. Iwayama, N. Sisourat, P. Lablanquie, F. Penent, J. Palaudoux, L. Andric, J.H.D. Eland, K. Bucar, M. Zitnik, Y. Velkov, Y. Hikosaka, M. Nakano and E. Shigemasa, *J. Chem. Phys.*, 2013, **138**, 024306-1-6.

37 S. Nagaoka, H. Fukuzawa, G. Prmper, M. Takemoto, O. Takahashi, K. Yamaguchi, T. Kakiuchi, K. Tabayashi, I. H. Suzuki, J. R. Harries, Y. Tamenori and K. Ueda, *J. Phys. Chem. A*, 2011, **115**, 8822-8831.

38 S. Nagaoka, G. Prmper, H. Fukuzawa, M. Hino, M. Takemoto, Y. Tamenori, J. Harries, I.H. Suzuki, O. Takahashi, K. Okada, K. Tabayashi, X-.J. Liu, T. Lischke and K. Ueda, *Phys. Rev. A*, 2007, **75**, 020502-1-4.

39 K. Le Guen, M. Ahmad, D. Colin, P. Lablanquie, C. Miron, F. Penent, P. Morin and M. Simon, *J. Chem. Phys.*, 2005, **123**, 084302-1-8.

40 C. Miron, M. Simon, N. Leclercq, D.L. Hansen and P. Morin, *Phys. Rev. Lett.*, 1998, **81**, 4104-4107.

41 A. Mocellin, K. Wiesner, S.L. Sorensen, C. Miron, K. Le Guen, D. Céolin, M. Simon, P. Morin, A.B. Machado, O. Björneholm, A. Naves de Brito, *Chem. Phys. Lett.*, 2007, **435**, 214-218.

42 H. Fukuzawa, G. Pruemper, X.-J. Liu, E. Kukk, R. Sankari, M. Hoshino, H. Tanaka, Y. Tamenori and K. Ueda, *Chem. Phys. Lett.*, 2007, **436**, 51-56.

43 E. Itälä, D.T. Ha, K. Kooser, M.A. Huels, E. Rachlew, E. Nmmiste, U. Joost and E. Kukk, *J. Electron Spectrosc. Relat. Phenom.*, 2011, **184**, 119-124.

44 R.R. Blyth, R. Delaunay, M. Zitnik, J. Krempasky, R. Krempaska, J. Slezak, K.C. Prince, R. Richter, M. Vondracek, R. Camilloni, L. Avaldi, M. Coreno, G. Stefani, C. Furlani, M. De Simone, S. Stranges and M.-Y. Adam, *J. Electron Spectrosc. Relat. Phenom.*, 1999, **101-103**, 959-964.

45 M. Lavollée, *Rev. Sci. Instrum.*, 1999, **70**, 2968-3974.

46 M. Alagia, P. Candori, S. Falcinelli, K.C. Mundim, M.S.P. Mundim, F. Pirani, R. Richter, S. Stranges and F. Vecchiocattivi, *Chem. Phys.*, 2012, **398**, 134-141.

47 D. Healion, H. Wang and S. Mukamel, *J. Chem. Phys.*, 2011, **134**, 124101-1-16.

48 J.H.D Eland, *Laser Chem.*, 1991, **11**, 259-263.

49 M. Alagia, P. Candori, S. Falcinelli, F. Pirani, M.S.P. Mundim, R. Richter, M. Rosi, S. Stranges and F. Vecchiocattivi, *Phys. Chem. Chem. Phys.*, 2011, **13**, 8245-8250.

50 S. Yang and R. Bersohn, *Phys. Chem. Chem. Phys.*, 1974, **61**, 4400-4407.

51 M. Alagia, C. Callegari, P. Candori, S. Falcinelli, F. Pirani, R. Richter, S. Stranges and F. Vecchiocattivi, *J. Chem. Phys.*, 2012, **136**, 204302-1-6.

52 http://cccbdb.nist.gov/